symmetry

MDPI

Article

Model-Free Generalized Super-Twisting Fast Terminal Sliding Mode Control for Permanent Magnet Synchronous Motors

Xingyi Ma, Yu Xu, Lei Zhang and Jing Bai *

College of Electrical and Information Engineering, Beihua University, Jilin 132021, China; senorito777@outlook.com (X.M.); jixuyu@beihua.edu.cn (Y.X.); 22110464@bjtu.edu.cn (L.Z.)
* Correspondence: jlbyj@beihua.edu.cn

Abstract: Permanent Magnet Synchronous Motors (PMSMs) are nonlinear, multi-parameter systems that exhibit structural symmetry but are susceptible to parameter variations and external disturbances. These challenges can disrupt the inherent symmetrical characteristics of PMSM dynamics during real-world operations, posing difficulties for achieving efficient control. To address this issue, this paper proposes a Model-Free Generalized Super-Twisting Algorithm Fast Terminal Sliding Mode Control (MFFTSMC-GSTA) method. First, a novel ultra-local model incorporating PMSM uncertainties is established, and the MFFTSMC-GSTA controller is designed to address the system's complex dynamic behavior. By integrating the generalized super-twisting algorithm with the nonsingular fast terminal sliding mode algorithm, the proposed controller ensures finite-time convergence and effectively mitigates chattering. Second, an extended sliding mode disturbance observer is developed to estimate the unknown components of the ultra-local model and provide feedforward compensation, further enhancing system robustness and dynamic performance. The experimental results show that the total harmonic distortion (THD) value of the proposed control method is 1.38%, demonstrating significant improvements in response speed and robustness for motor speed control, and verifying the algorithm's superior performance under complex operating conditions.

Keywords: permanent magnet synchronous motor; model-free control; generalized super-twisting; nonsingular terminal sliding mode; extended sliding mode disturbance observer

check for updates

Academic Editors: Alexander Zaslavski and Quanxin Zhu

Received: 25 November 2024
Revised: 18 December 2024
Accepted: 23 December 2024
Published: 26 December 2024

Citation: Ma, X.; Xu, Y.; Zhang, L.; Bai, J. Model-Free Generalized Super-Twisting Fast Terminal Sliding Mode Control for Permanent Magnet Synchronous Motors. *Symmetry* **2025**, *17*, 18. https://doi.org/10.3390/sym17010018

Copyright: © 2024 by the authors. Licensee MDPI, Basel, Switzerland. This article is an open access article distributed under the terms and conditions of the Creative Commons Attribution (CC BY) license (https://creativecommons.org/licenses/by/4.0/).

1. Introduction

As global environmental issues become increasingly severe, the application of new energy technologies has gained prominence, with the development of new energy vehicles emerging as a focal point in the automotive industry. PMSMs are widely employed in automobiles due to their compact size and low noise levels. PMSMs are nonlinear, highly coupled, and multi-parameter complex systems. Traditional Proportional-Integral (PI) controllers are susceptible to disturbances and variations in motor internal parameters [1]. In recent years, various control methods for PMSMs have been proposed by researchers worldwide, including Active Disturbance Rejection Control (ADRC) [2,3], Adaptive Control [4,5], Fuzzy Control [6,7], and Sliding Mode Control (SMC) [8,9]. Among these, SMC has been widely used in PMSM control for its strong robustness, minimal sensitivity to parameter variations, and fast response speed [10]. However, while linear sliding mode control achieves asymptotic convergence, fast terminal sliding mode control (FTSMC) can achieve fast convergence in finite time but suffers from the singularity problem. FTSMC resolves the singularity issue while ensuring finite-time convergence. A major drawback of

SMC is chattering, caused by the inherent switching characteristics of the control. High-frequency switching in SMC maintains the system state on the sliding surface but leads to frequent oscillations near the surface, resulting in chattering. Moreover, the robustness of the discontinuous control term against external disturbances and system uncertainties can further exacerbate chattering. To address this issue, replacing the sign function in SMC with a hyperbolic tangent function achieves control continuity but introduces steady-state error [11]. Other approaches, such as Dynamic Sliding Mode Control [12], filtering methods [13], and Continuous Sliding Mode Control [14], have been proposed, but these methods often compromise system performance to some extent. The Super-Twisting Algorithm (STA) is an improved high-order sliding mode control method that embeds the sign function for high-frequency switching into the higher-order derivatives of the sliding mode variable, effectively reducing chattering. Additionally, STA incorporates an integral term in the switching component of the control law. This effectively suppresses high-frequency chattering caused by sliding mode switching [15]. In recent years, more researchers have combined STA with FTSMC, leveraging the chattering reduction capability of STA and the fast convergence performance of TSMC to enable the system's rotational speed to quickly reach the target state [16]. However, for high-precision control applications, STA-based FTSMC may fall short. Introducing an integral term into FTSMC can effectively improve tracking accuracy and enhance system robustness [17]. However, these methods rely heavily on accurate mathematical models. In practice, the uncertainties in motor parameters and the complex dynamic variations make precise modeling of motors challenging.

Model-free control (MFC) achieves efficient control of PMSM through real-time data feedback without relying on an accurate motor model. It accommodates the nonlinearity and parameter variations of PMSMs, providing strong disturbance rejection and adaptability, making it suitable for maintaining stable and efficient control in complex or uncertain environments. This approach simplifies controller design and parameter tuning processes [18]. By establishing an ultra-local model, MFC dynamically estimates the system's local behavior in real time through observations of input–output relationships [19]. The combination of MFC and SMC provides robustness and disturbance rejection without requiring a precise system model, making it suitable for complex and nonlinear systems. However, its drawbacks include potentially lower control accuracy and susceptibility to chattering [20]. In [21], a combination of MFC and Nonsingular Terminal Sliding Mode Control (NTSMC) was proposed, reducing dependence on system parameters and improving robustness and response speed. In [22], an improved novel integral fast terminal sliding mode control method was introduced, effectively mitigating the effects of unknown disturbances but showing limited effectiveness in suppressing chattering.

This paper proposes a MFFTSMC-GSTA method for PMSM drive systems based on an extended sliding mode disturbance observer. A novel ultra-local model is employed, combining model-free control with the Generalized Super-Twisting Fast Terminal Sliding Mode Control to design the MFFTSMC-GSTA. The extended sliding mode disturbance observer accurately estimates the unknown components of the ultra-local model and provides timely feedforward compensation to the MFFTSMC-GSTA, effectively improving the speed regulation system's robustness, responsiveness, and chattering suppression.

The structure of this paper is organized as follows: Section 1 introduces the background and motivation for this research, outlining the challenges in SPMSM speed control and the contributions of the proposed method. Section 2 provides the theoretical foundations that support the proposed control strategy. Section 3 details the design of the MFFTSMC-GSTA and the ESMDO. Section 4 presents simulation experiments to validate the dynamic performance and robustness of the proposed method. Section 5 further veri-

fies the practical application of the control strategy through experimental testing. Finally, Section 6 summarizes the main research findings and outlines future research directions.

2. System Model

2.1. PMSM Model

The mathematical equations for PMSM operating under ideal conditions are

$$\begin{cases} u_q = |R_s i_d| + |L_d|\frac{di_d}{dt}| - |\omega_e L_q i_q \\ u_q| = |R_s i_q| + |L_q|\frac{di_q}{dt}| + |\omega_e\,(|L_d i_d| + |\psi_f\,) \\ \frac{d\omega_e}{dt}| = |\frac{n_p}{J}\,(|T_e| - |T_L| - |B\omega_m|\,) \\ T_e| = |\frac{3}{2} n_p \psi_f i_q \end{cases} \tag{1}$$

where u_d is the stator d-axis voltage component, u_q is the stator q-axis voltage component, i_d is the stator d-axis current component, i_q is the stator q-axis current component, L_d is the d-axis inductance of the stator winding, L_q is the q-axis inductance of the stator winding, ω_e is the electrical angular velocity, B is the damping coefficient, T_e is the electromagnetic torque, J is the moment of inertia, T_L is the load torque, ω_m is the mechanical angular velocity, ψ_f is the permanent magnet flux linkage, R_s is the stator resistance, and n_p is the number of pole pairs.

Considering the impact of complex operating conditions on the stability of the system, the mathematical model of SPMSM under such conditions can be further expressed as follows [23]:

$$\begin{cases} u_d| = |R_\mathrm{s} i_d| + |L_d|\frac{\mathrm{d}i_d}{\mathrm{d}t}| - |\omega_\mathrm{e} L_q i_q| + |\Delta u_d \\ u_q| = |R_\mathrm{s} i_q| + |L_q|\frac{\mathrm{d}i_q}{\mathrm{d}t}| + |\omega_\mathrm{e}(|L_d i_d| + |\psi_\mathrm{f}|)| + |\Delta u_q \\ \frac{\mathrm{d}\omega_\mathrm{e}}{\mathrm{d}t}| = |\frac{n_\mathrm{p}}{J}(|T_\mathrm{e}| - |T_\mathrm{L}| - |B\omega_\mathrm{m}|)| + |\Delta P_\mathrm{n} \\ T_\mathrm{e}| = |\frac{3}{2} n_\mathrm{p} \psi_\mathrm{f} i_q| + |\Delta T_\mathrm{e} \end{cases} \tag{2}$$

where Δu_d is the d-axis voltage disturbance under complex operating conditions, Δu_q is the q-axis voltage disturbance under complex operating conditions, ΔT_e is the electromagnetic torque disturbance under complex operating conditions, and ΔP_n is the disturbance caused by variations in the moment of inertia J and damping coefficient B. By combining Equations (1) and (2), the following can be obtained:

$$\frac{d\omega_e}{dt} = \begin{bmatrix} \frac{3n_p^2}{2J}\psi_f i_q - \frac{B}{J}\omega_e + \\ \\ \frac{n_p}{J}(\Delta T_e - T_L + \Delta T_L) + \Delta P_n \end{bmatrix} \tag{3}$$

2.2. Ultra-Local Model of the Speed Loop for SPMSM

An ultra-local model is a simplified control model that dynamically estimates system behavior in real time without relying on an accurate mathematical model of the system. This approach is particularly effective for systems with significant uncertainties. The ultra-local model of a first-order nonlinear system can be expressed as follows:

$$\begin{cases} \dot{x} = g(x) + \lambda_1 u \\ y = x \end{cases} \tag{4}$$

where $x \in K, \lambda_1 \in K$ are the constant gain to be designed.

To establish a novel ultra-local model, $g(x)$ in Equation (4) is expressed as

$$g(x) = \lambda_2 x + F \tag{5}$$

where λ_2 is the system state gain to be designed, and F represents the unknown part.

By combining Equations (4) and (5), a novel ultra-local model for the speed loop can be established:

$$\begin{cases} \dot{x} = \lambda_2 x + F + \lambda_1 u \\ y = x \end{cases} \tag{6}$$

To ensure that the speed controller maintains high control performance under SPMSM parameter perturbations and time-varying disturbances, express x in Equation (6) as ω_e, and combine it with Equation (3). Treat $\frac{n_p}{J}(\Delta T_e - T_L + \Delta T_L) + \Delta P_n$ in Equation (3) as the unknown disturbance F. The speed loop ultra-local model is then designed as follows:

$$\begin{cases} \left|\frac{d\omega_e}{dt}\right| = |\lambda_1 i_q| + |\lambda_2 \omega_e| + |F \\ \left|\frac{dF}{dt}\right| = |\Lambda(|t|) \end{cases} \tag{7}$$

where $\lambda_1 = 3n_p^2\psi_f/2J, \lambda_2 = -B/J, \Lambda(t)$ represents the rate of change of F. Based on Equations (3) and (7), Equation (8) is designed as

$$\left|i_q^*\right| = \left|\frac{\left|\dot{\omega}_e^*\right| - |\lambda_2 \omega_e| - |F| + |u_c}{\lambda_1}\right| \tag{8}$$

where $u_{|c|}$ is the control law to be designed.

3. Improved Model-Free Generalized Super-Twisting Nonsingular Fast Terminal Sliding Mode Control (MFFTSMC-GSTA)

The improved MFFTSMC-GSTA primarily consists of two parts:

(1) Design of the MFFTSMC-GSTA reaching law: This combines the Generalized Super-Twisting Algorithm (GSTA) and Fast Terminal Sliding Mode Control (FTSMC) to design the reaching law for MFFTSMC-GSTA, with its stability and reachability proven.

(2) Design of the Extended Sliding Mode Disturbance Observer (ESMDO): The block diagram of the PMSM speed control system using MFFTSMC-GSTA and ESMDO is shown in Figure 1.

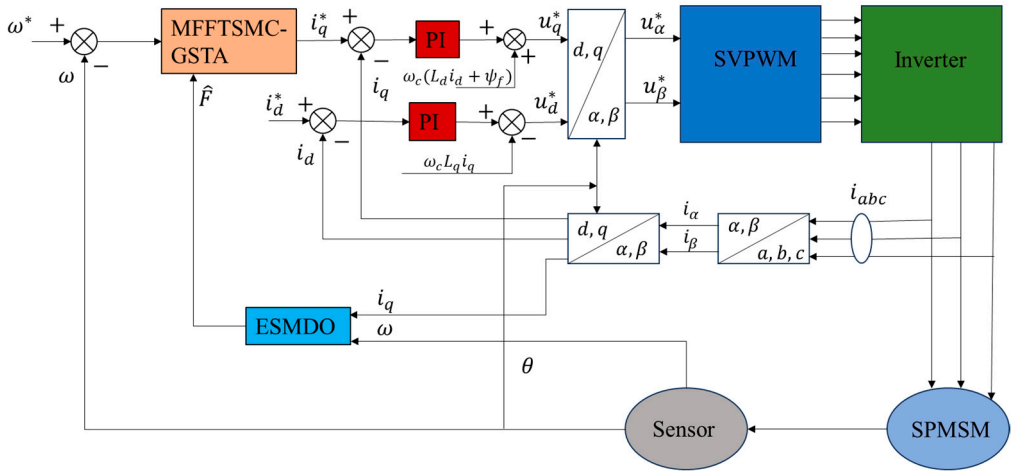


Figure 1. The PMSM Speed Control System Based on MFFTSMC-GSTA.

3.1. Design of the MFFTSMC-GSTA Controller

Define the state error as

$$e| = |\omega_e^*| - |\omega_e \tag{9}$$

By combining Equations (7)–(9):

$$\dot{\omega}_e^* - \dot{\omega}_e| = -|u_c \tag{10}$$

For Equation (10), the NFTSM sliding surface ss is designed as

$$s = C_1 e + \dot{e} + C_2 |e|^{\frac{q}{p}} sgn(e) \tag{11}$$

where C_1 and C_2 are positive constants to be designed, and q, p are odd numbers to be determined.

For the speed error Equation (10), selecting the second-order fast terminal sliding surface defined in Equation (11), the system state will converge rapidly in finite time once it enters the fast terminal sliding surface.

Taking the derivative of Equation (11) and choosing an exponential reaching law, substituting the state Equation (7) yields

$$\begin{aligned} \dot{s} &= C_1 \dot{e} + \ddot{e} + C_2 |e|^{\frac{q}{p}-1} \dot{e} \\ &= -k_1 sign(s) - k_2 s \end{aligned} \tag{12}$$

where k_1, k_2 are constant values. From Equation (7), it follows that $\frac{d\omega_e}{dt}| = |\lambda_1 i_q| + |\lambda_2 \omega_e| + |F$, i.e., $-\dot{e} = \dot{\omega}_e$. Therefore, Equation (13) is obtained.

$$\ddot{e} = -\left(\lambda_1 \dot{i_q}| + |\lambda_2 \dot{\omega}_e| + |\dot{F}\right) \tag{13}$$

By combining Equations (7) and (13), the following can be obtained:

$$i_q^* = \int \frac{-\left(k_1 sign(s) + k_2 s + C_1 \dot{e} + C_2 |e|^{\frac{q}{p}-1} - \lambda_2 \dot{e} - \dot{F}\right)}{\lambda} d\tau \tag{14}$$

To prove the stability of Equation (13), the Lyapunov function is designed as $V_1 = \frac{1}{2} s^2$, resulting in

$$\begin{aligned} \dot{V} &= s\dot{s} \\ &= s\left(\ddot{e} + \left(\dot{\omega}_e^* - F - \alpha u_c - \beta \omega_e\right)\left(C_1 + C_2 |e|^{\frac{q}{p}-1}\right)\right) \\ &= s(-k_1 sign(s) - k_2 s) \\ &\leq -k_1 |s| - k_2 s^2 \end{aligned} \tag{15}$$

According to Equation (15), when k_1 and k_2 are chosen as appropriate positive gain values, the error can converge to zero in finite time, ensuring system stability.

From Equation (14), it can be observed that i_q^* contains a discontinuous sign function, which inevitably induces high-frequency chattering in the system, adversely affecting both dynamic and static performance. The STA mitigates chattering by incorporating a discontinuous function with a large gain into the integral term $\int \vartheta_2 sign(s) dt$. However, the convergence speed of this algorithm primarily depends on the proportional term $\vartheta_1 \sqrt{|s|} sign(s)$, which is insufficient to handle disturbances effectively.

GSTA is an improved sliding mode control algorithm that introduces a continuous control input to effectively suppress chattering while ensuring fast convergence of the

system state. Therefore, this paper adopts the GSTA with an acceleration factor, which is expressed as follows:

$$\dot{s} = -\vartheta_1\sqrt{|s|}sign(s) - \lambda_1 s + \rho_1 - \int (\vartheta_2 sign(s) + \lambda_2 s + \rho_2)dt \tag{16}$$

When ρ_1, ρ_2 satisfy the below equation:

$$\begin{cases} |\rho_1| \leq \gamma_1\sqrt{|s|} + \gamma_2|s| \\ |\rho_2| \leq \gamma_3 + \gamma_4|s| \end{cases} \tag{17}$$

where $\gamma_1, \gamma_2, \gamma_3, \gamma_4 \geq 0$. As shown in Equation (17), when the parameters in the controller are appropriately selected, the system is guaranteed to converge to the sliding surface in finite time. The detailed proof can be found in [24]:

$$\begin{cases} \vartheta_1 > 2max\left(\gamma_1, \sqrt{\gamma_3}\right) \\ \vartheta_2 > max\left(\vartheta_1 \frac{\gamma_1\vartheta_1 + \frac{1}{8}\gamma_1^2 + \gamma_3}{2\left(\frac{1}{2}\vartheta_1 - \gamma_1\right)}\right. \\ \qquad \frac{\left(\lambda_1\gamma_1 + \frac{1}{2}\vartheta_1\gamma_2\right)^2}{2\lambda_1(\lambda_1 - 2\gamma_2)} + \\ \qquad \left.\frac{\left(\delta_3 + \frac{3}{2}\vartheta_1\delta_1\right)\lambda_1 - 2\left(\lambda_1 - \frac{1}{4}\delta_2\right)\vartheta_1^2}{(\lambda_1 - 2\delta_2)}\right) \\ \lambda_1 > max\left(\frac{3}{8}\gamma_3 + \frac{1}{4}\sqrt{\frac{9}{4}\gamma_3^2 + 8\gamma_4}, |2\gamma_3\right) \\ \lambda_2 > max\left(\lambda_1 \frac{\left[\lambda_1(\lambda_1 + 3\gamma_2) + \frac{1}{2}\gamma_2^2 + \gamma_4\right]}{\lambda_1 - 2\gamma_2},\right. \\ \qquad \frac{\vartheta_1\left[\frac{1}{2}\vartheta_1\left(\vartheta_1 + \frac{1}{3}\gamma_1^2\right)\left(2\lambda_1^2 - \frac{3}{3}\gamma_2\lambda_1 - \gamma_4\right)\right]}{2\left(p_1 - \frac{1}{2}\vartheta_1\left(\vartheta_1 + \frac{1}{2}\gamma_1\right)^2\right)\left(\frac{1}{2}\vartheta_1 - \gamma_1\right)} + \\ \qquad \left.\frac{\vartheta_1\left[\left(\frac{5}{2}{\lambda_1}^2 + \frac{3}{2}\gamma_2\lambda_1 + \gamma_4\right)p_1\right]}{2\left(p_1 - \frac{1}{2}\vartheta_1\left(\vartheta_1 + \frac{1}{2}\gamma_1\right)^2\right)\left(\frac{1}{2}\vartheta_1 - \gamma_1\right)}\right. \end{cases} \tag{18}$$

where $p_1 \triangleq \vartheta_1\left(\frac{1}{4}\vartheta_1^2 - \gamma_3\right) + \left(\frac{1}{2}\vartheta_1 - \gamma_1\right)\left(2\vartheta_2 + \frac{1}{2}\vartheta_1^2\right)$. Based on Equations (13) and (15), the control law is given as follows:

$$i_q^* = \int \frac{-\left(\vartheta_1\sqrt{|s|}sign(s) + \lambda_1 s + \int(\vartheta_2 sign(s) + \lambda_2 s)dt + C_1\dot{e} + C_2|e|^{\frac{q}{p}-1} - \lambda_2\dot{e} - \dot{F}\right)}{\lambda} d\tau \tag{19}$$

To prove the stability of Equation (18), the Lyapunov function is designed as $V_1 = \frac{1}{2}s^2$, resulting in

$$\begin{aligned} \dot{V} &= s\dot{s} \\ &= s\left(\ddot{e} + \left(\dot{\omega_e^*} - F - \alpha u_c - \beta\omega_e\right)\left(C_1 + C_2|e|^{\frac{q}{p}-1}\right)\right) \\ &= s\left(-\vartheta_1\sqrt{|s|}sign(s) - \lambda_1 s - \int(\vartheta_2 sign(s) + \lambda_2 s)dt\right) \\ &= -\vartheta_1|s|^{\frac{3}{2}} - \lambda_1 s^2 - s\int(\vartheta_2 sign(s) + \lambda_2 s)dt \\ &\leq -\vartheta_1|s|^{\frac{3}{2}} - \lambda_1 s^2 \end{aligned} \tag{20}$$

When the values of ϑ_1 and λ_1 satisfy Equation (17), the error can converge to zero in finite time, ensuring system stability.

The block diagram of the designed MFSTFTSMC-GSTA algorithm is shown in Figure 2.

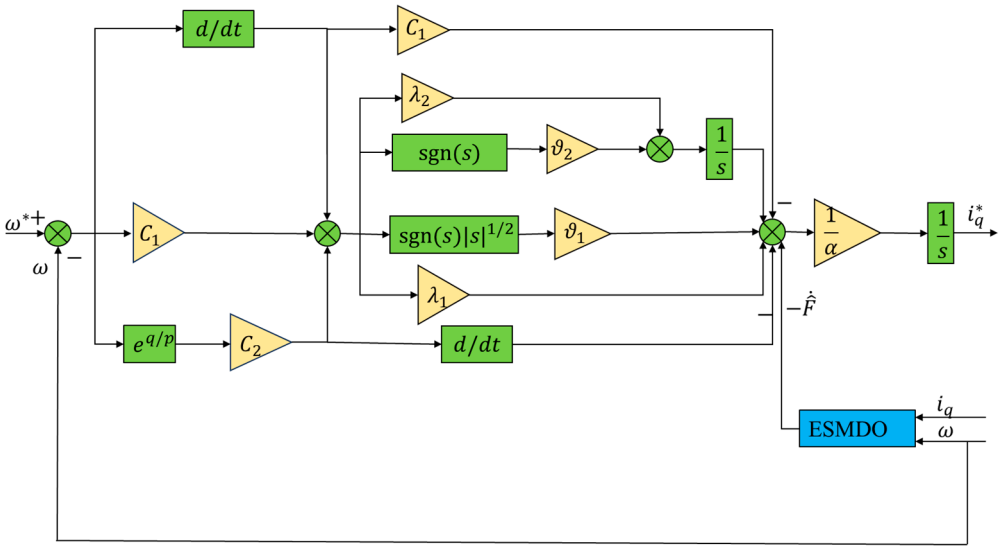


Figure 2. Block diagram of MFSTFTSMC-GSTA algorithm.

3.2. Design of the ESMDO

From the equation, it is known that the system has an unknown disturbance F. An Extended Sliding Mode Disturbance Observer (ESMDO) can be designed to accurately estimate the unknown disturbance. Based on Equation (7), the extended ultra-local model for the speed loop is expressed as

$$\begin{cases} \frac{d\omega_e}{dt}| = |\lambda_1 i_q| + |\lambda_2 \omega_e| + |F| \\ \frac{dF}{dt}| = |\tau| \end{cases} \tag{21}$$

where τ represents the rate of change of the unknown disturbance.

For the system in Equation (19), design an ESMDO as shown in the following equation:

$$\begin{cases} \frac{d\hat{\omega}_e}{dt}| = |\lambda_1 i_q| + |\lambda_2 \hat{\omega}_e| + |\hat{F} + u| \\ \frac{d\hat{F}}{dt}| = |\varepsilon \cdot u| \end{cases} \tag{22}$$

where $\hat{\omega}_e$ is the observed value of the rotational speed, $\hat{F}$ is the real-time estimation of the unknown part of the system, u is the sliding mode control law, and $\varepsilon > 0$ is the gain of the observer.

$$\begin{cases} \dot{e}_\omega = \eta e_\omega + e_f + u \\ \dot{e}_f = \varepsilon \cdot u - w(t) \end{cases} \tag{23}$$

where e_ω is the speed estimation error, $e_\omega = \hat{\omega}_e - \omega_e . e_f$ is the observation error of the unknown disturbance, $e_f = \hat{F} - F$.

The sliding surface is chosen as

$$s_1 = \hat{\omega}_e - \omega_e \tag{24}$$

The constant sliding mode reaching law is chosen as

$$\dot{s}_1 = -Msign(s) \tag{25}$$

From Equations (22) and (23), the control law for the ESMDO is obtained as

$$u| = -|\lambda_2 s_1| - Msign(s) \tag{26}$$

To verify the stability of the observer, the Lyapunov function is designed as $V_1 = \frac{1}{2}s_1^2$, resulting in

$$\begin{aligned} \dot{V} &= s_1 \dot{s}_1 \\ &= s_1 (\dot{\hat{\omega}}_e - \dot{\omega}_e) \\ &= s_1 (-Msign(s)) \\ &\leq -Ms_1^2 \end{aligned} \tag{27}$$

When M is chosen as an appropriate positive gain, the system is guaranteed to converge in finite time.

$$\hat{F}| = |\varepsilon| \int (| - |\lambda_2 s_1| - Msign(s)|)|dt \tag{28}$$

Substituting Equation (22) into Equation (18), the overall control law i_q^* for the controller is obtained as follows:

$$i_q^* = \int \frac{-(\vartheta_1 \sqrt{|s|} sign(s) + \lambda_1 s + \int (\vartheta_2 sign(s) + \lambda_2 s)dt + C_1 \dot{e} + C_2 |e|^{\frac{q}{p}-1} - \lambda_2 \dot{e} - \dot{\hat{F}})}{\lambda} d\tau \tag{29}$$

The block diagram of the designed ESMDO algorithm is shown in Figure 3.

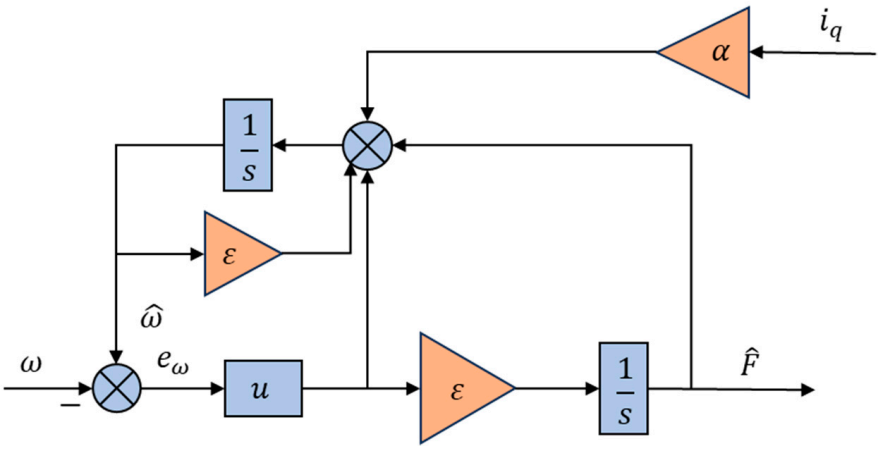


Figure 3. Block diagram of ESMDO algorithm.

4. Simulation

To verify the effectiveness of the designed controller in a high-performance vector control system, simulations were conducted using the MATLAB/SIMULINK 22a platform. The performance of the proposed controller has been compared with MFFTSMC, MFFTSMC-STA, MFFTSMC-GSTA, and MFFTISMC. MFFTISMC originates from the study presented in reference [25]. The reaching law of the literature [25] is

$$\dot{s} = -\wp |s|^v sign(s) - \Im f(s), f(s) = \begin{cases} s & |s| \leq u \\ sign(s) & |s| > u \end{cases} \tag{30}$$

where $\wp$, $\Im$, and u are the constants; $1 > v > 0$.

Details of the SPMSM parameters and related controller parameters are provided in Tables 1 and 2. The vector control system adopts SVPWM.

Table 1. SPMSM parameters.

Parameters	Values
Number of pole-pairs	4
Stator resistance	1.9275 Ω
Stator inductance (d-q axes)	3.2×10^{-3} H
Permanent magnet flux linkage	0.1218 Wb
Inertia	2.45×10^{-4} kg m^2
Viscous damping	0.001 N·m·s

Table 2. Controller parameters.

MFFTSMC	$c_1 = 0.2$; $c_2 = 20$; $k_1 = 3$; $k_2 = 180$; $q = 1$; $p = 3$
MFFTSMC-STA	$c_1 = 37$; $c_2 = 5$; $q = 1$; $p = 3$; $\lambda = 580$; $\alpha = 23$
MFFTSMC-GSTA	$c_1 = 42$; $c_2 = 3$; $\lambda_1 = 4$; $\vartheta_1 = 638$; $\lambda_2 = 1$; $\vartheta_2 = 20,000$; $q = 1$; $p = 3$;
MFFTSMC-ISMC	$c_1 = 35$; $c_2 = 7$; $v = 1$, $u = 1$, $\wp = 600$, $\Im = 50$;

The system starts at a set speed of 400 RPM in a no-load startup mode. At 1 s, the speed increases to 600 RPM, followed by a load increase of 0.5 N·m at 2 s. At 3 s, the speed decreases to 500 RPM. Subsequently, at 4 s, the load decreases by 0.4 N·m, and at 5 s, the flux linkage ψ_f changes from 0.128 Wb to 0.15 Wb, and the inertia changes from 2.45×10^{-4} kg·m^2 to 2.55×10^{-4} kg·m^2. The speed, a-phase current, and total harmonic distortion (THD) are shown in Figures 4 and 5.

From Figure 4a, it can be observed that MFFTSMC demonstrates a rapid response to speed changes during no-load startup. However, as shown in Figure 4c, this control strategy exhibits slower recovery times and notable disturbances during steady-state operation under external perturbations, which result in reduced overall stability. For instance, in Figure 4d, the system requires an extended duration to return to its desired operational state following a sudden increase in load.

In contrast, MFFTSMC-STA exhibits a faster response speed, as illustrated in Figure 4b during acceleration. When disturbances occur, such as the sudden decrease in load shown in Figure 4f, this method responds promptly, enabling the system to restore steady-state conditions within a shorter timeframe. However, this rapid response comes at the expense of larger speed variations, leading to significant fluctuations when handling disturbances, as observed in Figure 4e,h, which may adversely affect the system's smooth operation.

The MFFTSMC-GSTA method offers improvements over these two approaches. It preserves the attributes of second-order sliding mode control while incorporating an integral term to further reduce system chattering. This integral term effectively accumulates error information, enhancing disturbance rejection and improving steady-state performance. Moreover, the MFFTSMC-GSTA method achieves a balance between responsiveness and stability, as demonstrated in Figure 4c,g. It not only reacts swiftly to disturbances with a short recovery time, as depicted in Figure 4d, but also minimizes speed fluctuations during steady-state operation. The chattering performance of different control methods during steady-state operation is presented in Table 3.

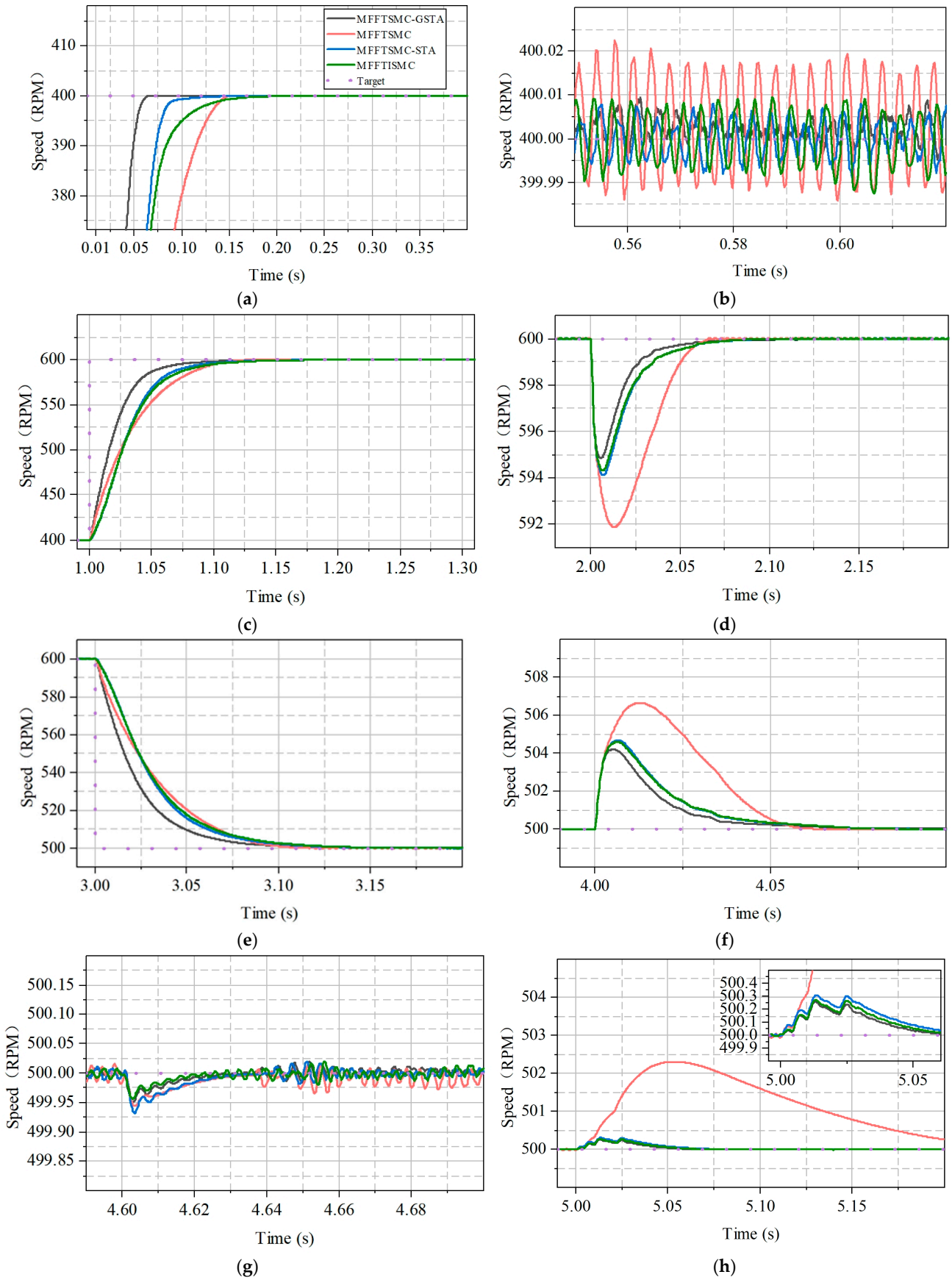


Figure 4. The speed response: (**a**) No-load startup; (**b**) Acceleration; (**c**) Acceleration; (**d**) Sudden increase of 0.5 N·m load; (**e**) Deceleration; (**f**) Sudden decrease of 0.5 N·m load; (**g**) Flux change; (**h**) Inertia changes.

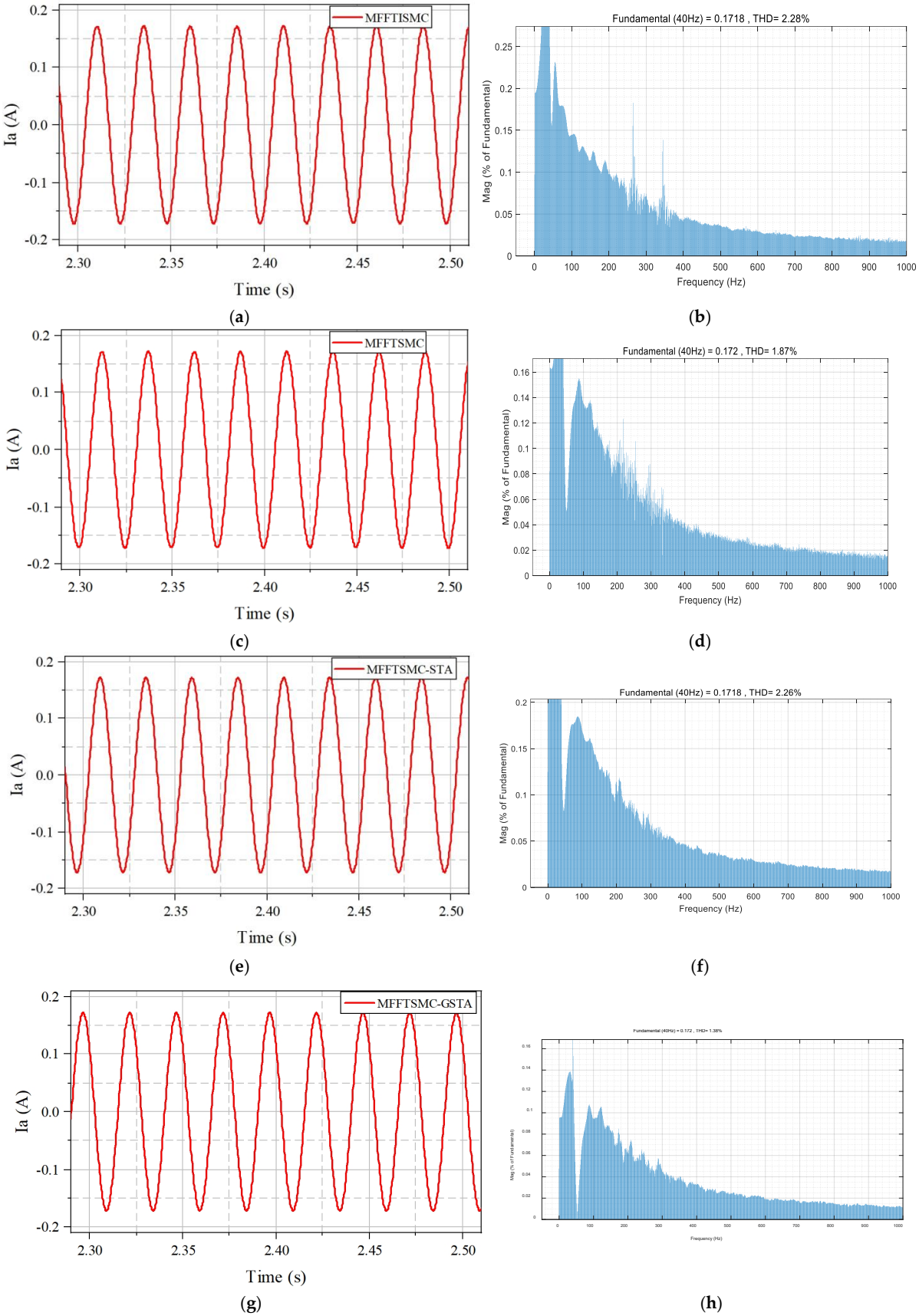


Figure 5. The A-axis current and THD: (**a**) A-axis current of the MFFTISMC; (**b**) THD of the MFFTISMC; (**c**) A-axis current of the MFFTSMC; (**d**) THD of the MFFTSMC; (**e**) A-axis current of the MFFTSMC-STA; (**f**) THD of the MFFTSMC-STA; (**g**) A-axis current of the MFFTSMC-GSTA; (**h**) THD of the MFFTSMC-GSTA.

Table 3. Analysis of Chattering Dynamics for Different Control Methods.

Control Methods	Amplitude of Chattering
MFFTSMC	0.02
MFFTSMC-STA	0.008
MFFTISMC	0.01
MFFTSMC-GSTA	0.005

Chattering is essentially caused by the high-frequency switching of the control signal, which introduces high-frequency components into the system's output signal. These high-frequency components are not part of the motor or system's normal operating frequencies but are instead harmonic distortions generated by the switching behavior in SMC. These components directly affect the motor's current and speed responses, resulting in increased THD. In traditional SMC, the switching function (e.g., $sign(s)$) is inherently discontinuous, containing an infinite spectrum of high-frequency components. While this characteristic enables rapid convergence to the sliding surface, the high-frequency components can excite the system dynamics, leading to pronounced chattering due to the physical limitations of actuators and equipment.

In contrast, the GSTA effectively mitigates chattering through several mechanisms. First, the nonlinear reaching law term ($-\vartheta_1\sqrt{|s|}sign(s)$) introduces a power-based modulation mechanism that slows the convergence rate as the error sss decreases, thereby avoiding the abrupt and high-frequency switching associated with traditional SMC. Specifically, the $\sqrt{|s|}$ term ensures a smoother convergence behavior, while ϑ_1 controls the intensity of the convergence rate. Second, the integral adjustment term ($-\int(\vartheta_2 sign(s)+\lambda_2 s)dt$) provides a dynamic regulation mechanism by accumulating error information to buffer and smooth out oscillations. This integral action not only suppresses the high-frequency components caused by switching but also dynamically compensates for disturbances, enhancing the system's robustness and disturbance rejection capability. Additionally, the linear reaching term ($-\lambda_1 s$) contributes to stabilizing the control behavior by providing a linear convergence characteristic, effectively reducing the likelihood of high-frequency chattering.

Overall, GSTA achieves smoother control signals and significantly reduces the high-frequency switching characteristics of traditional SMC through the combined effects of the nonlinear reaching law, linear adjustment term, and integral regulation term. This design not only diminishes the amplitude of chattering but also reduces the harmonic components in the system's output, thereby achieving a significant reduction in THD. By retaining the rapid convergence advantages of sliding mode control while suppressing high-frequency oscillations, GSTA provides a balanced solution for improving both the dynamic response and steady-state performance of the system, making it a highly effective approach for mitigating chattering and reducing harmonic distortion.

The THD analysis of the A-phase current, as shown in Figure 5a–h, reveals that the THD values for MFFTISMC, MFFTSMC, MFFTSMC-STA, and MFFTSMC-GSTA are 2.28%, 1.87%, 2.26%, and 1.38%, respectively. This demonstrates that the proposed MFFTSMC-GSTA effectively suppresses current harmonics compared to MFFTISMC, MFFTSMC, and MFFTSMC-STA.

5. Experimental Validation

To verify the effectiveness of the proposed control algorithm, physical experiments were conducted. The experimental platform, as shown in Figure 6, consists of a personal computer, a DSP control platform, a PMSM, a dynamic torque sensor, and an oscilloscope. The DSP control platform used is the MwSim-DSP-PMSM1.0, manufactured in Suzhou, China, and the PMSM model is SDGA-02C11BD manufactured in Shenzhen, China.

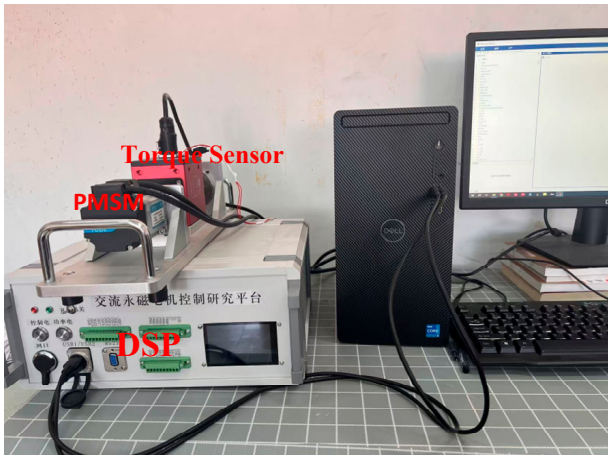


Figure 6. Experimental platform.

For the real system, the parameters of the MFFTSMC were adjusted to $C1 = 1$ and $C2 = 50$. For the other three control methods, $C1$ and $C2$ were set to 40 and 5, respectively, while the remaining parameters were consistent with the simulation. The parameter adjustment was designed to account for the dynamic characteristics of the actual system, including potential non-ideal factors such as inverter nonlinearity and component variations, to better reflect the algorithm's real-world performance.

To further validate the proposed algorithm, the experiment involved increasing the motor speed from 400 rpm to 1000 rpm, with a load torque of 1 N·m applied. To ensure the reliability and authenticity of the results, the oscilloscope recordings (Figures 7–9) illustrate the experimental outcomes of the four control methods under conditions of no-load startup, load application, and speed increase.

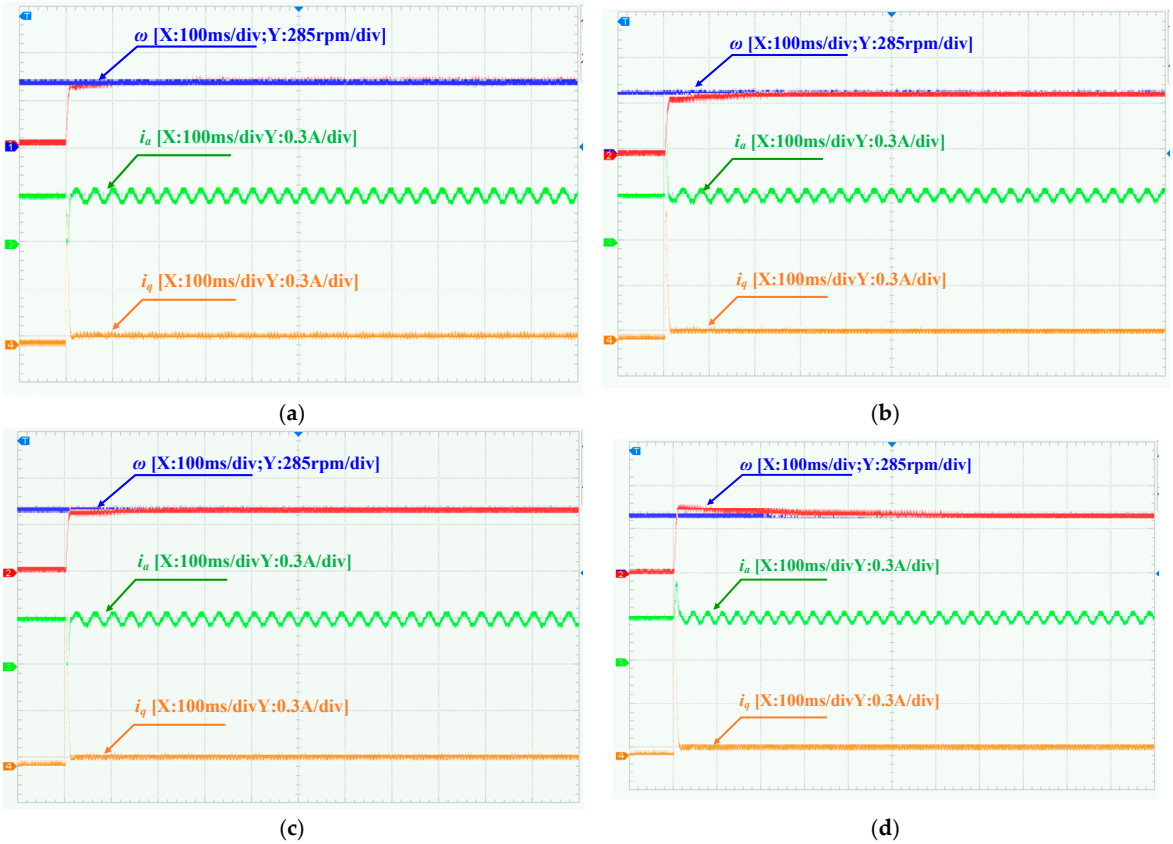


Figure 7. No-load startup: (**a**) MFFTSMC-GSTA; (**b**) MFFTSMC-STA; (**c**) MFFTISMC; (**d**) MFFTSMC.

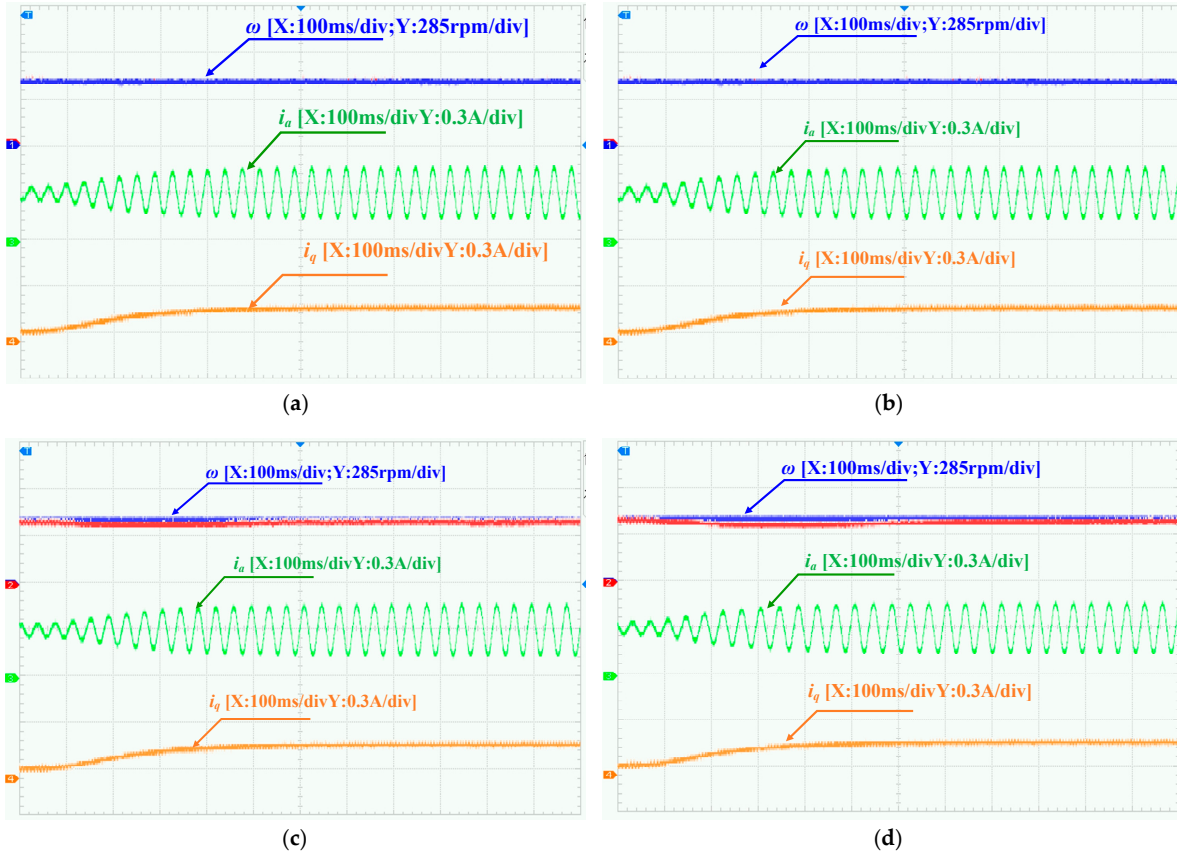


Figure 8. Load application: (**a**) MFFTSMC-GSTA; (**b**) MFFTSMC-STA; (**c**) MFFTISMC; (**d**) MFFTSMC.

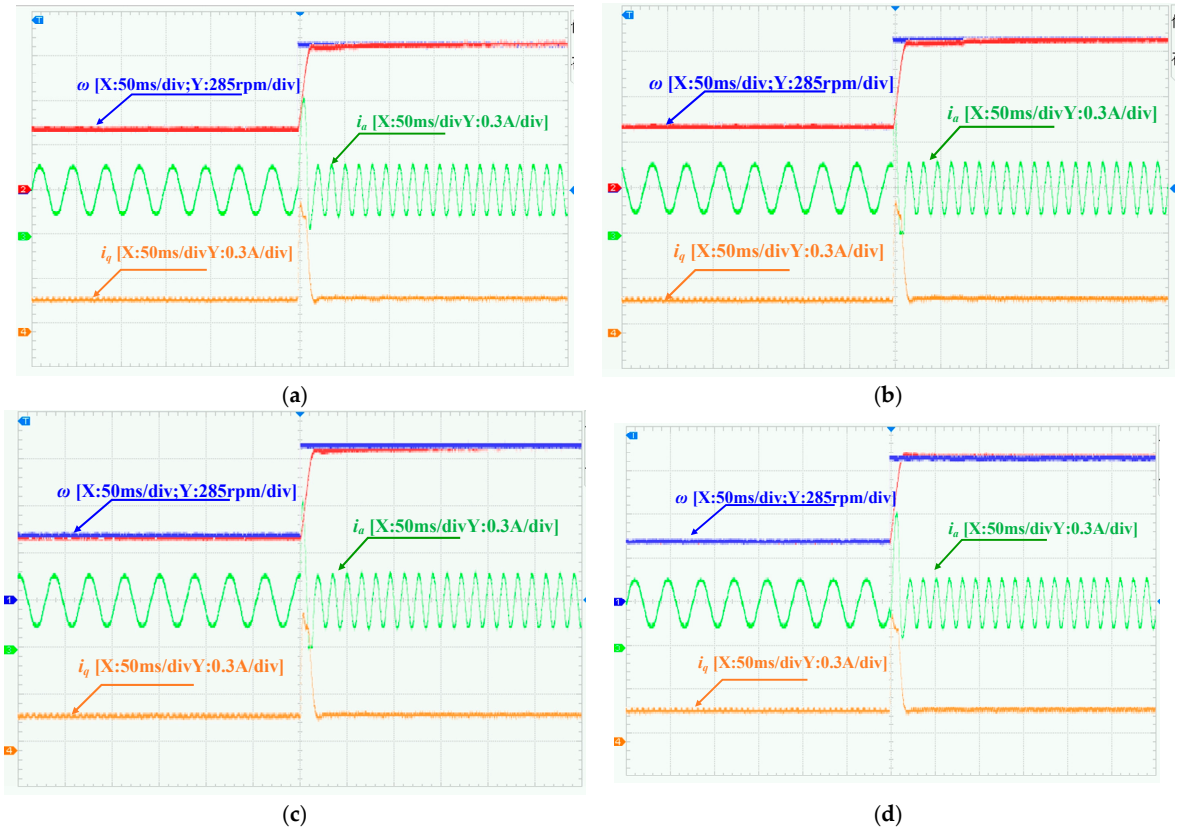


Figure 9. Speed increase: (**a**) MFFTSMC-GSTA; (**b**) MFFTSMC-STA; (**c**)MFFTISMC; (**d**) MFFTSMC.

Figure 7 illustrates the speed response during the no-load startup phase for different control methods. The MFFTSMC-GSTA method demonstrates the fastest response time of 4 ms, showcasing excellent dynamic performance. In contrast, the MFFTSMC-STA and MFFTSMC methods require 12 ms to complete the startup, while the MFFTISMC method has the slowest response time of 14 ms. Additionally, the MFFTSMC and MFFTISMC methods exhibit significant fluctuations during the startup process, whereas the MFFTSMC-GSTA and MFFTSMC-STA methods maintain smoother speed curves.

Figure 8 depicts the speed variation under a load disturbance of 1 N·m. The MFFTSMC-GSTA method exhibits the smallest speed fluctuation of 5.7 rpm and quickly returns to steady state, demonstrating exceptional disturbance rejection capability. The MFFTSMC-STA and MFFTISMC methods exhibit speed fluctuations of 7.5 rpm and 17.1 rpm, respectively, with the latter showing a notably weaker ability to handle disturbances. In comparison, the MFFTSMC method experiences the largest speed fluctuation of 28.5 rpm, indicating lower system stability.

Figure 9 presents the acceleration performance when increasing speed from 400 rpm to 1000 rpm. The MFFTSMC-GSTA method completes the acceleration in 10 ms, maintaining system stability without noticeable overshoot. In comparison, the MFFTSMC-STA and MFFTISMC methods require 12 ms and 14 ms, respectively, to achieve the target speed, showing relatively weaker dynamic performance. While the MFFTSMC method completes acceleration in 15 ms, it exhibits significant speed fluctuations during the process, negatively impacting overall performance. The specific vibration values for different control methods are shown in Table 4.

Table 4. Control Performance Comparison of Different Control Methods.

Control Method	Response Time (No-Load Startup, ms)	Speed Variation After Load Disturbance (rpm)	Response Time (Acceleration, ms)
MFFTSMC-GSTA	4	5.7	10
MFFTSMC-STA	12	7.5	12
MFFTISMC	14	17.1	14
MFFTSMC	12	28.5	15

The experimental results demonstrate that the MFFTSMC-GSTA method exhibits significant performance advantages under various operating conditions. During the no-load startup phase, this method achieves a response time of only 4 ms, which is markedly faster than other control methods, showcasing excellent dynamic response performance. Under a load of 1 N·m, the speed fluctuation of the MFFTSMC-GSTA method is limited to 5.7 rpm, highlighting its superior disturbance rejection capability. In the acceleration process, the MFFTSMC-GSTA method completes the speed increase from 400 rpm to 1000 rpm within 10 ms, maintaining stability without noticeable overshoot. Overall, the experimental results confirm that the MFFTSMC-GSTA method outperforms other control methods in terms of response speed, disturbance rejection, and dynamic stability, providing strong evidence of the proposed algorithm's effectiveness and superiority in motor speed control applications.

6. Conclusions

To achieve high-performance control of the SPMSM speed control system under internal and external disturbances, this paper proposes an MFFTSMC-GSTA strategy. Through comparisons with MFFTSMC and MFFTSMC-STA, the following conclusions are drawn:

(1) Chattering Suppression and Finite-Time Convergence: By combining GSTA with FTSMC, the proposed strategy effectively suppresses chattering while ensuring finite-time convergence, achieving superior dynamic performance and stability.
(2) Disturbance Estimation and Improved Robustness: The introduction of ESMDO enables real-time estimation of internal uncertainties and external disturbances, significantly enhancing the system's robustness. When the motor system is subjected to parameter variations and load disturbances, the proposed strategy allows the motor speed to quickly recover to a stable state, improving speed response and robustness performance.
(3) Dynamic and Static Performance Advantages: Compared with MFFTSMC and MFFTSMC-STA, the proposed strategy demonstrates stronger robustness under parameter variations and load disturbances while exhibiting superior dynamic response and steady-state performance.
(4) Practical Applications and Generalizability: Due to its model-free nature, the proposed strategy does not rely on the accurate mathematical model of the system, making it adaptable to other nonlinear systems with uncertainties and disturbances. Furthermore, the control strategy features low computational demand, making it suitable for real-time applications. It has significant practical value in industrial scenarios such as high-performance motor drive systems, robotic servo control, and electric vehicle drives.

Author Contributions: Conceptualization, X.M. and L.Z.; methodology, X.M.; software, X.M.; validation, Y.X., J.B. and L.Z.; formal analysis, X.M.; writing—original draft preparation, X.M.; writing—review and editing, L.Z. and J.B. All authors have read and agreed to the published version of the manuscript.

Funding: This research was funded by Jilin Provincial Department of Science and Technology, China, grant number 20230204093YY.

Data Availability Statement: The data used to support the findings of this study are available from the corresponding author upon request.

Conflicts of Interest: The authors declare no conflicts of interest.

Abbreviations

u_d, u_q	d- and q-axes stator voltage (V)
i_d, i_q	d- and q-axes stator current (A)
ψ_f	permanent magnet flux linkage (Wb)
L_d, L_q	d- and q-axes nominal stator inductances (H)
ω_e	electrical angular velocity (rad/s)
J	moment of inertia (kg m^2)
R_s	stator resistance (Ω)

References

1. Zhang, L.; Bai, J.; Wu, J. SPMSM Sliding Mode Control Based on the New Super Twisting Algorithm. *Complexity* **2021**, *2021*, 2886789. [CrossRef]
2. Hou, Q.; Zuo, Y.; Sun, J.; Lee, C.H.T.; Wang, Y.; Ding, S. Modified nonlinear active disturbance rejection control for PMSM speed regulation with frequency domain analysis. *IEEE Trans. Power Electron.* **2023**, *38*, 8126–8134. [CrossRef]
3. Zhang, X.; Chen, Y.; Sun, X. Overview of active disturbance rejection control for permanent magnet synchronous motors. *J. Electr. Eng. Technol.* **2024**, *19*, 1237–1255. [CrossRef]
4. Suganthi, S.; Karpagam, R. Dynamic performance improvement of PMSM drive using fuzzy-based adaptive control strategy for EV applications. *J. Power Electron.* **2023**, *23*, 510–521. [CrossRef]
5. Bai, Y.; Zhang, L.; Meng, X.-M.; Bai, J.; Han, G. A Novel Terminal Sliding Mode Variable Structure Model Reference Adaptive System Observer for Permanent Magnet Synchronous Motors. *Int. Trans. Electr. Energy Syst.* **2024**, *2024*, 4528374. [CrossRef]

6. Wang, Z.; Yu, A.; Li, X.; Zhang, G.; Xia, C. A Novel Current Predictive Control Based on Fuzzy Algorithm for PMSM. *IEEE J. Emerg. Sel. Top. Power Electron.* **2019**, *7*, 990–1001. [CrossRef]
7. Guo, Q.; Han, J.; Peng, W. PMSM Servo Control System Design Based on Fuzzy PID. In Proceedings of the 2017 2nd International Conference on Cybernetics, Robotics and Control (CRC), Chengdu, China, 21–23 July 2017; pp. 85–88. [CrossRef]
8. Zhang, L.; Sun, C.; Ma, Y.; Huang, J. An Improved Sliding Mode Model Reference Adaptive System Observer for PMSM Applications. *Expert Syst. Appl.* **2024**, *250*, 123907. [CrossRef]
9. Yang, R.; Wang, M.; Li, L.; Zenggu, Y.; Jiang, J. Integrated uncertainty/disturbance compensation with second-order sliding-mode observer for PMLSM-driven motion stage. *IEEE Trans. Power Electron.* **2019**, *34*, 2597–2607. [CrossRef]
10. Kim, C.; Kim, T.; Lyou, J. Robust Speed Control of a PMSM through Sliding Mode Controller Design. In Proceedings of the 2011 IEEE Symposium on Industrial Electronics and Applications, Langkawi, Malaysia, 25–28 September 2011; pp. 30–35. [CrossRef]
11. Lee, T.H.; Tan, K.K.; Huang, S. Adaptive Friction Compensation with a Dynamical Friction Model. *IEEE/ASME Trans. Mechatron.* **2011**, *16*, 133–140. [CrossRef]
12. Kavikumar, R.; Lee, S.-H.; Sakthivel, R.; Kwon, O.-M. Fuzzy dynamic sliding mode control for permanent magnet synchronous generator model. In Proceedings of the 2023 23rd International Conference on Control, Automation and Systems (ICCAS), Yeosu, Republic of Korea, 17–20 October 2023; pp. 1215–1220. [CrossRef]
13. Lin, F.J.; Hsieh, H.J.; Chou, P.H. Tracking Control of a Two-Axis Motion System via a Filtering Type Sliding Mode Control with Radial Basis Function Network. *IET Control Theory Appl.* **2010**, *4*, 655–671. [CrossRef]
14. Wang, F.; Wei, Y.; Young, H.; Ke, D.; Xie, H.; Rodríguez, J. Continuous-control-set model-free predictive fundamental current control for PMSM system. *IEEE Trans. Power Electron.* **2023**, *38*, 5928–5938. [CrossRef]
15. Li, Z.; Zhou, S.; Xiao, Y.; Wang, L. Sensorless Vector Control of Permanent Magnet Synchronous Linear Motor Based on Self-Adaptive Super-Twisting Sliding Mode Controller. *IEEE Access* **2019**, *7*, 44998–45011. [CrossRef]
16. Zhao, Z.; Gu, H.; Zhang, J.; Ding, G. Terminal Sliding Mode Control Based on Super-Twisting Algorithm. *J. Syst. Eng. Electron.* **2017**, *28*, 145–150. [CrossRef]
17. Ma, Y.; Li, D.; Li, Y.; Yang, L. A Novel Discrete Compound Integral Terminal Sliding Mode Control with Disturbance Compensation for PMSM Speed System. *IEEE/ASME Trans. Mechatron.* **2022**, *27*, 549–560. [CrossRef]
18. Zhou, Y.; Li, H.; Yao, H. Model-Free Control of Surface-Mounted PMSM Drive System. In Proceedings of the 2016 IEEE International Conference on Industrial Technology (ICIT), Taipei, Taiwan, 14–17 March 2016; pp. 175–180. [CrossRef]
19. Zhao, K.; Liu, W.; Yin, T.; Zhou, R.; Dai, W.; Huang, G. Model-Free Sliding Mode Control for PMSM Drive System Based on Ultra-Local Model. *Energy Eng.* **2022**, *119*, 767–780. [CrossRef]
20. Ebrahimi, N.; Ozgoli, S.; Ramezani, A. Model-Free Sliding Mode Control, Theory and Application. *Proc. Inst. Mech. Eng. Part I J. Syst. Control Eng.* **2018**, *232*, 1292–1301. [CrossRef]
21. Zhao, K.; Yin, T.; Zhang, C.; He, J.; Li, X.; Chen, Y.; Zhou, R.; Leng, A. Robust Model-Free Nonsingular Terminal Sliding Mode Control for PMSM Demagnetization Fault. *IEEE Access* **2019**, *7*, 15737–15748. [CrossRef]
22. Zhao, K.; Liu, W.; Zhou, R.; Dai, W.; Wu, S.; Qiu, P.; Yin, Y.; Jia, N.; Yi, J.; Huang, G. Model-Free Fast Integral Terminal Sliding-Mode Control Method Based on Improved Fast Terminal Sliding-Mode Observer for PMSM with Unknown Disturbances. *ISA Trans.* **2023**, *143*, 572–581. [CrossRef] [PubMed]
23. Zhang, L.; Tao, R.; Zhang, Z.-X.; Chien, Y.-R.; Bai, J. PMSM Non-Singular Fast Terminal Sliding Mode Control with Disturbance Compensation. *Inf. Sci.* **2023**, *642*, 119040. [CrossRef]
24. Moreno, I.; Osorio, M. A Lyapunov Approach to Second-Order Sliding Mode Controllers and Observer. In Proceedings of the IEEE Conference on Decision and Control, Cancun, Mexico, 9–11 December 2008; pp. 2856–2861.
25. Zhao, K.; Dai, W.; Zhou, R. A novel model-free sliding mode control for permanent magnet synchronous motor based on extended sliding mode disturbance observer. *Proc. CSEE* **2022**, *42*, 2375–2386.

Disclaimer/Publisher's Note: The statements, opinions and data contained in all publications are solely those of the individual author(s) and contributor(s) and not of MDPI and/or the editor(s). MDPI and/or the editor(s) disclaim responsibility for any injury to people or property resulting from any ideas, methods, instructions or products referred to in the content.